

Elucidating Deep Reservoir Geometry and Lateral Outflow Through 3-D Elastostatic Modeling of Satellite Radar (InSAR) Observed Surface Deformations: An Example From the Bradys Geothermal Field

Gary Oppliger¹, Mark Coolbaugh², Lisa Shevenell² and James Taranik¹

¹Arthur Brant Laboratory for Exploration Geophysics, UNR

²Great Basin Center for Geothermal Energy, UNR

Keywords

Reservoir characterization, subsidence modeling, InSAR, interferometry, radar, ground-water hydrology

ABSTRACT

Utilizing the Bradys geothermal field as a case example, we demonstrate a new approach for modeling satellite interferometric synthetic aperture radar (InSAR) observed surface deformations in terms of 3-D subsurface volume-strain rate (change) distributions. The approach allows us to interactively model the 3-D subsurface volume-strain distributions subject to geologic constraints and leads to enhanced geometric interpretability of InSAR patterns over the Bradys field. A key result is the recognition of volume-strain in shallow lateral horizons to the northwest of the Bradys field. It appears that these lateral strain horizons are a significant part of the InSAR response and that they must be modeled in combination with the reservoir system to arrive at plausible geometries for the reservoir.

Introduction

We develop a new methodology for interpreting satellite interferometric synthetic aperture radar (InSAR) observed deformation in terms of 3-D subsurface volume-strain distributions and apply it to modeling the Bradys geothermal reservoir system. A key conclusion derived from the model is that changes in temperature and/or pressure in upper lateral outflow zones make a significant contribution to the observed InSAR patterns and must be modeled in combination with the operational reservoir.

InSAR for Geothermal Reservoir Monitoring

Surface deformation will occur as a consequence of the production of geothermal fluids even if the reservoir is deep and isolated from shallow groundwater (Vasco et al., 2002).

Reservoir deformation is largely driven by temperature and pressure reductions. Where coupling into a shallow groundwater aquifer occurs, the surface deformation response will contain additional elements (Poland, 1984). These include volume-strain from the newly added weight of deposits that have lost buoyant support, and the simple dehydration shrinkage of clayey deposits. Because all of the above effects are typically associated with production and are centered on the most permeable structures they are not easily separable. Use of additional data, such as ground-water levels and reservoir modeling, may help determine their relative significance in a particular case.

Repeat-orbit differential Interferometric Synthetic Aperture Radar (InSAR) was introduced thirteen years ago as an operational research technology with the launch of the European Space Agency's (ESA) ERS 1 satellite. InSAR has been utilized for its ability to image earth surface deformation related to earthquakes, volcanic intrusions, and the production of groundwater, geothermal energy and petroleum (Massonet, 1998). InSAR is a surface displacement change detection method with unprecedented millimeter level sensitivity. Surface displacements that occur in the time interval between the acquisitions of two radar scenes are inferred by comparing the differences in travel times of radar waves at discrete points within the surface radar image. This is accomplished by combining the two radar scenes to form an interferogram or phase interference image. InSAR offers two distinct advantages over traditional optical leveling and GPS for vertical surface change detection. First it can provide map-like images at resolutions of 20-40 meters covering 100 km by 100 km regions. Second, it can be applied in retrospective change studies by using the 12 year archive of ERS 1/2 scenes.

InSAR's ability to monitor surface deformation at geothermal fields has been well established on some of the larger fields (e.g., Coso: Fialko and Simons, 2000) and models for inversion of reservoir volume-strain have been developed and applied (Vasco et al., 2002). Oppliger et.al. (2004) also describe an example of InSAR's application over the 26.1 MWe Bradys geothermal field.

Lateral Geothermal Fluid Flow and Linkages to Bedrock Aquifers

Convective flow processes are generally accepted as responsible for the upward transport of thermal energy and fluids from several kilometers depth in geothermal systems localized by high-angle fault systems. For convective flow to continue, fluid must escape from confining vertical conduits and enter other available permeable horizons (or reach the surface). This outflow is eventually confined from further vertical movement by overlying impermeable horizons or by simply reaching the level of the water table. At that point outflow is driven only by the hydrothermal cell's elevated central pressure field.

With regard to the Bradys field area, Harrill (1970) describes likely basin-scale groundwater flow towards Bradys Hot Springs as occurring as subsurface flow from the northwest and also possibly from the southwest. Further, surface observables show groundwater discharge from the thermal area is by evapotranspiration and lateral subsurface outflow toward the south. The natural preproduction state of the Bradys geothermal field also included convective up-flow as evidenced by its historic hot spring flows and fumaroles (Benoit, 1982) which could potentially supply horizontal outflow. Downward increasing temperatures in drill-holes several kilometers peripheral to the Bradys field indicate this outflow is occurring at depth rather than just at the surface. This allows the possibility that both the reservoir and outflow systems could experience production related perturbations in temperature, pressure and flows rates that may be expressed in InSAR observations. This paper focuses on isolating and modeling these two separate geometric signal sources at the Bradys geothermal field.

The Benefits Derived from Understanding the Lateral Outflow

From a geothermal field management perspective, understanding changes in the lateral outflow volumes and patterns might appear to be of little importance. Lateral outflow generally has a much lower temperature than fluid produced at depth, and it is exiting the field. So what can be gained by observing it? First, by accounting for lateral outflow's contribution to the InSAR pattern, the reliability of reservoir geometric modeling can be improved. Second, since flow barriers (impermeable faults) channel the outflow, changes to flow rates may reveal these structures. Third, part of the outflow may contribute to the field's short-term self-recharge by becoming downward convective return flow in distal segments of the Bradys fault. Hence, understanding these patterns may allow improved placement of reinjection wells to optimize the resource.

The Modeling Method

To develop the example used in this paper we started by forming 35 interferograms from 18 ERS 1 & 2 raw SAR radar scenes with 1 to 9 year intervals using JPL's ROI_PAC processing package. From these a subset of high quality, low atmospheric noise interferograms were selected for conver-

sion from observed phase patterns to millimeters of local ground displacement and further processing. Even the best of these interferograms contained some areas of localized phase decorrelation and data dropouts (noise) over key areas of the geothermal field. This problem occurs when the centimeter-scale textural patterns of surface reflectors are altered significantly in a group of adjacent image pixels. ROI_PAC's phase unwrapping algorithm automatically masks those areas as being too ambiguous for algorithm treatment. We have found we can reliably connect gaps in the unwrapped phase contours by overlaying the machine unwrapped version on the original interferogram and drawing in a few representative contours to complete the reconstruction. We then employ minimum curvature interpolation to generate a continuous deformation surface for further processing.

To remove the InSAR anomaly's directional asymmetry resulting from combined sampling of vertical and horizontal surface displacement fields along the satellite's 24 degree off-vertical line-of-sight (LOS) viewing angle, we apply elastic deformation theory to transform the LOS anomalies to apparent vertical deformation. (Oppliger, publication in preparation). We note that source modeling can be accomplished with or without transformation to the vertical with identical results, but we find it advantageous to be able to work with deformation maps and profiles in which anomaly asymmetry originates only from source-body asymmetry and not viewing angle.

Our interpretation of InSAR deformation patterns in terms of volume-strain sources carries with it an assumption that no significant percentage of the InSAR observed deformation field in the reservoir anomaly is contributed by strike or dip slip fault dislocations. We can reasonably conclude from several lines of evidence that slip dislocations are not significant contributors to the InSAR observations. Evidence includes the absence of major InSAR anomaly asymmetries required by the geometry of strike slip displacement and the absence of fresh strike-slip offsets and dip-slip scarps. Any significant contribution to the InSAR deformation observations would require recent ground fault displacements of at least several centimeters.

The next step utilizes the prepared InSAR observations to model the distribution of volume-change in the reservoir system. This requires implementing a mathematical relation (Green's response function) between a point element volume-strain and the elastostatic deformation field at the surface. For our Greens function we select the Mogi elastic half-space volume-strain source (Mogi, 1958).

With a focus on modeling volcanic intrusive activity, Mogi (1958) showed the vertical surface deformation Δh produced from inflation and deflation of a spherical cavity in an isotropic homogeneous elastic half-space is defined by:

$$\Delta h = \frac{3\Delta P V_r (1 - \nu)}{4\pi\mu} \frac{Z}{(Z^2 + X^2)^{3/2}} \quad (1)$$

where Z is the source depth, X is the horizontal distance from the source epicenter, ΔP is the pressure change, V_r is the volume of the source and ν and μ are the Poisson's ratio and shear modulus of the half-space media.

The pressure change ΔP can be related to a small volume change ΔV_r of the source spherical cavity sphere V_r through

$$\Delta V_r = \frac{3V_r \Delta P}{4\mu} \quad (1.2)$$

Eliminating this pressure term, Mogi's equation is rewritten in terms of pure volume-change as

$$\Delta h = \frac{\Delta V_r (1 - \nu)}{\pi} \frac{Z}{(Z^2 + X^2)^{3/2}} \quad (1.3)$$

This volume-change form of Mogi's equation is applicable to modeling InSAR observations in terms of their best-fitting subsurface source distributions. Analysis of the individual thermal and pressure contributions may follow the geometric source modeling.

Equation (1.3) shows the shear modulus of the homogeneous half-space's does not influence the solution but that Poisson's ratio does. Poisson's ratio, a measure of a materials compressibility or dilatancy under linear strain, induces additional volume-change inside and outside the reservoir, which contributes to the total change observed at surface. Johnson (1995) showed that Poisson's ratio in the surrounding material effectively amplifies the amount of volume-change observed at surface ΔV_e relative to that actually occurring in within the Mogi source ΔV_r by:

$$\Delta V_e = 2(1 - \nu)\Delta V_r \quad (1.4)$$

Employing a Poisson's ratio of 0.25, typical of sedimentary and volcanic strata, Equation 1.4 defines an amplification factor of 1.5.

A Mogi volume-change source produces an isotropic (radial) displacement field. Because the source strength is defined only as the delta volume-change rather than pressure, elastic material properties do not enter the equation provided they are uniform. Despite the simplistic assumption of uniform elastic properties in half-space, the Mogi-type source continues to find wide use in reservoir modeling applications. Generally no increase in model accuracy can be achieved with more complex Greens functions which incorporate variations in the elastic material properties (Poisson ratio and shear modulus) unless the property distributions are adequately known.

A second well studied choice of Greens function for an elastic half-space is a planar dislocation source (Okada, 1985, Wicks et al., 2001, Fialko and Simons, 2000). This represents the non-radial half-space displacement field associated with opening or closing of a tensile fracture. We suspect this volume-change mechanism may be important in some zones of the Bradys reservoir and will investigate this in future work. For the current work we use a Mogi source, as it is a good choice to represent the dominant isotropic thermoelastic and poroelastic effects.

Having selected a Green's function to characterize elastic deformation, we next describe our methodology for distributing it in the subsurface model volume. Previous approaches applying Mogi-type sources to geothermal deformation modeling have employed either a small number of individual point sources, multiple prolate spheroidal sources (Fialko and Simon,

2000), or 3-D grids of hundreds of point sources which act as a continuous volume-change field (Vasco et al., 2002). Our approach differs from these, by its use of uniform volume-strain (defined in parts per million or ppm) in interpreter definable 3-D prisms. In other words, specific reservoir zones, such as the reservoir's core area are allocated a constant volume-strain. However, both the assigned strain and its boundaries are modifiable. The actual numerical computation employed to forward calculate surface displacements is implemented using line integrals over the prism cross-sections using methods defined by Talwani (1964), as this is more efficient than a volume integration.

Using a graphical drawing interface linked to this elastic deformation forward calculation, a set of nested 3-D polygons representing known reservoir boundaries is built-out. The model's interactive graphical facility makes it possible to incorporate known thermal, hydrologic and geologic controls and the interpreter's insights, while the forward model calculation display provides the interpreter with immediate feedback to test his ideas. We have found that just the process of preparing a few models provides new insights into how the reservoir may be responding to production.

We note that our model solutions represent generic volume-strain. Volume-strain can be physically linked to temperature and pressure change when sufficient data are available to assign a distribution to at least one of these. The initial values of volume-strain for the starting model can be constrained to realistic ranges by applying the maximum down-hole temperature and pressure change observed in the reservoir's core. For example thermoelastic strain has typical values for rocks of 20-30 ppm volume-strain per °C change, so an initial guess for a reservoir core with 1°C/year drop would be 25 ppm of volume-strain. We may also calculate the possible poroelastic contributions to volume-strain from pressure reduction if estimates of the reservoir's shear or bulk modulus can be developed. See Mossop and Segall (1997) for an example of the uncertainties involved in estimating the effective bulk modulus for The Geysers geothermal reservoir in northern California. Since poroelastic strain estimates involve more assumptions and show greater variability than their thermoelastic counterparts we set the starting volume-strain value based on the available reservoir temperature change data. Since our model is not sensitive to the physical cause of the strain, we can experiment with separating the thermoelastic and poroelastic effects after the model is defined. If the starting model strain value is either too low or too high, it will be evident in the modeling process, and adjustments can be made to the zone's width or strength.

Discussion of Model Results

We experimented by producing a number of volume-strain rate models, each of which were in good agreement with the InSAR observations. We discuss one model result which is representative of the models produced. This model is presented in Figure 2 and was developed to fit InSAR observations extracted along line AA', in Figure 1. (Note, we included Desert Peak in the model for geographic continuity but its anomaly is

too weakly expressed to allow clear definition of its reservoir's geometry.)

We used the subsurface temperature isotherms and the dip of the Brady fault from Holt, et al.'s (2004) Bradys reservoir model to constrain the position of the reservoir core area. This core was modeled with a 28 ppm/year volume-strain rate, which is compatible with a 1 °C/year temperature change. Holt, et al.'s (2004) data suggest plant in-flow temperature decreases of about 1.2 °C/year. We then built-out a second zone with a 9 ppm/year rate to represent a halo zone around the core with a lower rate of temperature (0.33 °C/year) and pressure reduction. The northwest dip of the Bradys field only partly replicated the long wavelength anomaly in that direction. We found it necessary to add a significant northwest horizontal lobe on the reservoir at a depth between sea-level and the surface. We speculate that this volume-strain pattern may be produced from changes in geothermal fluid outflow into the upper adjacent aquifer system which result in minor temperature or pressure decreases.

The ~250 meter thick thermal aquifer in Figure 2 is in effect shrinking at a rate of 9 ppm/year which is consistent with a ~0.33 °C/year temperature reduction. If the effective aquifer model thickness were changed to 500 meters, the required temperature decrease would be only 0.150 °C/year. These numbers represent the maximum possible temperature change in their respective aquifer systems, because pore pressure decrease associated with reduced outflow almost certainly accounts for a portion of the aquifer volume loss.

Benoit (1982) describes well temperature log evidence that supports the existence of at least four near-surface thermal aquifers adjacent to the Desert Peak and Bradys fields; but notes the well data is far too incomplete to describe the aquifers spatial and depth extent. These thermal aquifers have been inferred largely by down-hole temperature reversals occurring in Tertiary volcanic and sedimentary units in the upper 500 meters lateral to the know fields. Around Desert Peak temperature reversals are most commonly documented in the upper 300-400 meters but are seen as deep as 1000 meters. The effective thickness of the known thermal aquifer, as defined by the length of the temperature reversals, range from 3 meters to 300 meters. Northwest of the Bradys field, 10 widely spaced temperature gradient wells of less than 150 meters depth define a northwest projecting lobe with elevated thermal gradients ranging from 3 to 6 °C over 30 meters depth. Although these anomalous gradients suggest a possible deeper thermal aquifer they fail to confirm it or eliminate the possibility of its existence due to their limited measurement depths.

Source Depth Ambiguity

It is well known that any observed surface deformation distribution can be reproduced, to

an arbitrary "goodness-of-fit" level, by an unlimited number of volume-strain distributions, one of which is confined to an arbitrarily thin layer just below the surface. This is the principle of source distribution equivalency that is also commonly encountered in geophysical potential field modeling. If unconstrained by sufficient physical considerations, no particular physical significance can be assigned to any particular model solution other than knowledge of its horizontal location and the total volume-change it represents. Fortunately, geologic, geophysical, geothermal and hydrologic considerations allow us to avoid physically unlikely volume-strain distributions and build models that are consistent with the geologic knowns and hydrothermal physics of a geothermal field. Nonetheless, available constraints may still allow a choice between representing the long wavelength (LWL) InSAR components as sourced in the shallow subsurface or at a depth of a few kilometers under the producing field.

For geothermal systems with suspected underlying deep active magmatic system (such as Coso) it is logical to assign the LWL features to deep sources. However, when geological, geophysical and geochemical data, provide no justification for a deep magmatic source, other physically probable volume-strain distributions must be considered. At the Bradys field, several

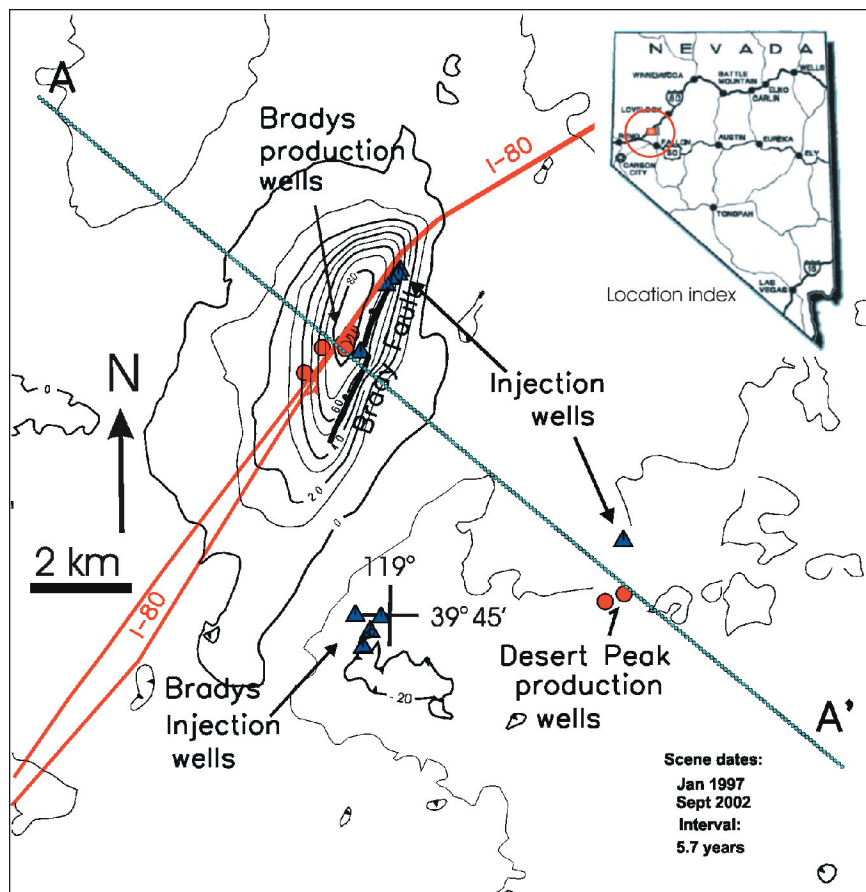


Figure 1. Plan map showing the Jan. 1997 to Sept. 2002 InSAR anomaly contoured at 10 mm intervals. The InSAR line-of-sight deformation has been transformed to vertical deformation in mm and filtered to remove signal from features with wavelengths less than 120 meters. Production and injection wells, Interstate Highway I-80, and model profile A-A' are shown for spatial reference.

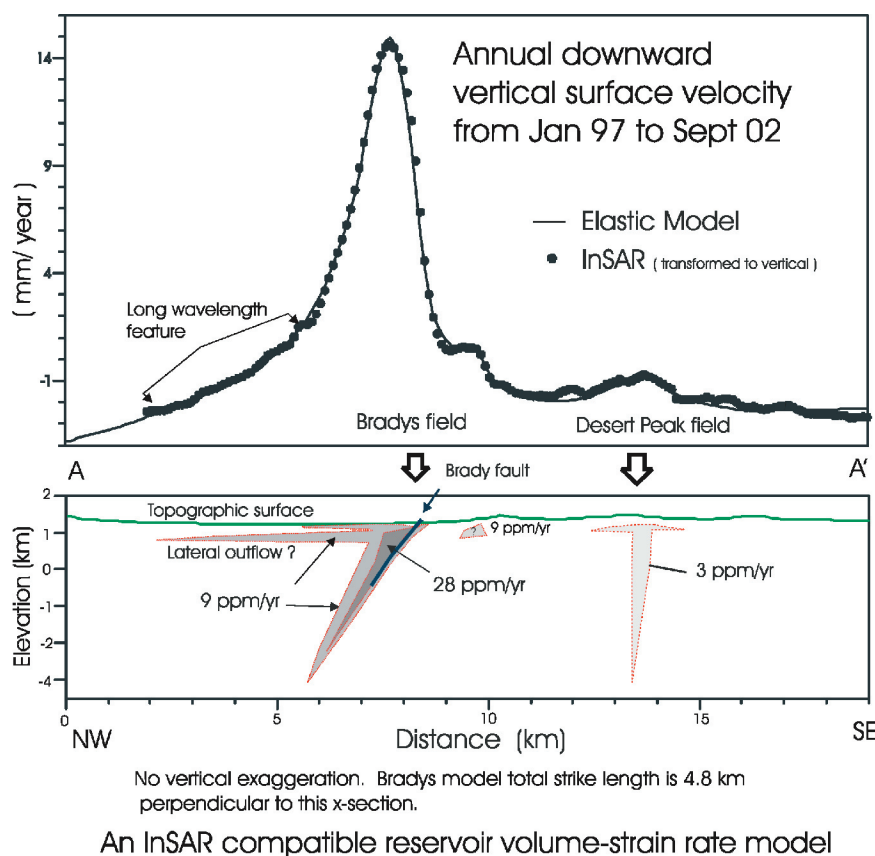


Figure 2. Model cross-section and InSAR anomaly along profile AA' showing an InSAR compatible volume-strain rate model for the Bradys and Desert Peak fields during the 5.7 year period from Jan. 1997 to Sept. 2002. The Bradys field anomaly is robustly resolved in the data, but the Desert Peak anomaly is too weak to yield reliably reservoir geometry details. The long wavelength surface deformation feature on the extreme left (northwest) part of the profile suggests significant volume-strain is occurring in that area somewhere between the surface and about 1.5 kilometers depth. The vertical surface displacements contoured in Figure 1 are divided by 5.7 years to define the vertical velocities in mm/year shown in this profile. The elastic model employs a Poisson's ratio of 0.25.

lines of evidence suggest the producing field is interacting with a relatively shallow (1.5 km depth) aquifer system around the geothermal field.

Similar LWL components are often seen in urban, agricultural and mine dewatering anomalies, which have no association with geothermal or active magmatic systems. When these features are modeled by single Mogi volume-strain point or spherical sources, model depths sometimes appear to be several times deeper than the known production depths. This effect reflects the influence of a layered aquifer system which is confining flow, pressure reduction and deformation within horizontal boundaries. The resulting horizontally broadened surface deformation pattern will appear to have a deeper source if the aquifer geometry is ignored in the modeling.

Most geothermal production involves a net extraction of fluid accompanied by lowered pressures in the reservoir environment; this situation has the potential to produce an analog to mine dewatering in the surrounding aquifer environment.

The Bradys field InSAR pattern contains a number of narrow width anomalies, which we interpret as caused by fault plane flow barriers. Since these narrow wavelengths require

sources in the upper 100-200 meters, it is clear that lateral outflow is occurring at this shallow level.

Conclusions

Our study shows the Bradys geothermal field is associated with a broad, 6 km wide, northwesterly skewed, vertical-component surface displacement anomaly which suggests minor volume loss in the range of a 9 to 28 ppm is occurring in the reservoir and surrounding aquifers. The anomaly's northwest projecting long wavelength asymmetry is not adequately modeled by a symmetric, dipping reservoir system aligned on the northwesterly dipping Bradys fault. An additional sub-horizontal tabular volume-strain source extending about 5 km northwest of the Brady reservoir in the upper 1.5 km is one physically plausible model solution that accounts for this long wavelength asymmetry. We speculate that this lateral tabular volume-strain feature is an indication of production induced change in the field's lateral outflow patterns which have resulted in small temperature and/or pressure reductions in these units. The results demonstrate it may be advantageous to include the volume-strain in the surrounding aquifer systems when modeling the geothermal reservoir. Although each geothermal field is unique, the ideas presented may have application to the modeling of other fields, in particular, as an alternative to exclusive use of deep magmatic sources to represent long wavelength InSAR anomalies.

Acknowledgements

This work was supported by the Department of Energy under DE-FG36-02ID14311 through the Great Basin Center for Geothermal Energy at UNR. Additional support was provided by the Arthur Brant Laboratory for Exploration Geophysics, University of Nevada Reno. JPL ROI_PAC v2.2.2 Repeat Orbit Interferometry radar processing software was utilized. Some of the raw ERS 1 & 2 radar scenes were provided by the WInSAR Consortium. Precise Orbits for the ERS 1 & 2 satellites were obtained from Delft Institute, The Netherlands.

References

- Benoit, W.R., Hiner, J.E., and Forest, R.T., 1982, Discovery and geology of the Desert Peak geothermal field: A case history: Nevada Bureau of Mines and Geology Bulletin 97, 82 p.
- Fialko, Y., and M. Simons, 2000, Deformation and seismicity in the Coso geothermal area, Inyo County, California: Observations and modeling using satellite radar interferometry, *Journal of Geophysical Research*, v. 105, p. 21,781-21,794.
- Harrill, J.R., 1970, Water-Resources Appraisal of the Granite Springs Valley Area, Pershing, Churchill, and Lyon Counties, Nevada: Nevada Department Conservation and National Resources, Water Resources-Reconnaissance Series Report 55, 36 p.

- Holt, R., Campbell, D. Matlick, S., 2004, Reservoir Simulation of Brady's Geothermal Field, Nevada, Geothermal Resources Council Transactions, v. 28, p. 589-593.
- Johnson, D.J., 1995, Gravity changes on Mauna Loa Volcano, in Mauna Loa Revealed: Structure, composition, History and Hazards, Geophysical Monograph 92, edited by J.M. Rhodes and John P. Lockwood, pp. 127-143, AGU, Washington, D.C..
- Massonnet, D. and Feigl, K. L., 1998, Radar interferometry and its application to changes in the earth's surface, Reviews of Geophysics, v. 36(4), p. 441-500.
- Mogi, K., 1958, Relations between the eruptions of various volcanoes and the deformations of the ground surface around them, Bull. Earthquake Res. Inst. Univ. Tokyo, v. 36, p. 99-134.
- Mossop, A., Segall, P., 1997, Subsidence at the Geysers geothermal field, N. California from a comparison of GPS and leveling surveys. Geophysical Research Letters, v 24, n 14, p 1839-1842.
- Okada, Y., 1985, Surface deformation due to shear and tensile faults in a half-space, Bull. Seis. Soc. Am., v. 75, 1135-1154.
- Oppliger, G., Coolbaugh, M. Foxall, W., 2004, Imaging Structure with Fluid Fluxes at the Bradys Geothermal Field with Satellite Interferometric Radar (InSAR): New Insights into Reservoir Extent and Structural Controls, v. 28, p. 27-40.
- Oppliger, G., in prep, Modeling full 3-D displacement fields directly from differential InSAR observations.
- Poland, J.F., 1984, Mechanics of land subsidence due to fluid withdrawal, in Poland, J.F., editor, Guidebook to studies of land subsidence due to ground-water withdrawal: Studies and Reports in Hydrology 40, UNESCO, p. 37-54.
- Talwani, M., and Heirtzler, J. R., 1964, Computation of magnetic anomalies caused by two-dimensional bodies of arbitrary shape, Computers in the mineral industries, Parks, G. A., (ed), School of Earth Sciences, Stanford University (Publication), p.464-480.
- Vasco D.W., Wicks, C., Jr., and Karasaki, K., 2002, Geodetic imaging: High-resolution reservoir monitoring using satellite interferometry, Geophysical Journal International, v. 149, p. 555-571.
- Wicks, C., Thatcher, W., Monastero, F., and Hasting, M., 2001, Steady-State Deformation of the Coso Range, East-Central California, Inferred from Satellite Radar Interferometry, Journal of Geophysical Research, v. 106, p. 13769 – 13780.